Journal Name

COMMUNICATION

Spontaneous power source in ambient air of a well-directionally reduced graphene oxide bulk †

Huhu Cheng,‡*[a,b] Yaxin Huang,‡[a] Fei Zhao,[e] Ce Yang,[a] Panpan Zhang,[a] Lan Jiang,[a,d] Gaoquan Shi§[b] and Liangti Qu*[a,c]

[a.] Key Laboratory for Advanced Materials Processing Technology, Ministry of Education of China; State Key Laboratory of Tribology, Department of Mechanical Engineering, Tsinghua University, Beijing 100084, PR China. E-mail: lqu@mail.tsinghua.edu.cn, huhucheng@tsinghua.edu.cn.
[b.] Department of Chemistry, Tsinghua University, Beijing 100084, PR China.
[c.] Beijing Key Laboratory of Photoelectronic/Electrophotonic Conversion Materials, School of Chemistry and Chemical Engineering, Beijing Institute of Technology, Beijing 100081, PR China.
[d.] Laser Micro-/Nano-Fabrication Laboratory, Beijing Institute of Technology, Beijing, 100081, PR China.
[e.] Materials Science and Engineering Program and Department of Mechanical Engineering, The University of Texas at Austin, TX, 78712, USA
†Electronic Supplementary Information (ESI) available. See DOI: 10.1039/x0xx00000x
‡These authors contributed equally.
§Deceased

Experimental Section

Preparation of a-GOM: Graphene oxide (GO) dispersion (~5 mg ml^{-1}) was prepared by modified Hummers' method.[s1,s2] After freeze-drying in a lyophilizer under 20 Pa for 12 h, a 10 cm^{-3} GO foam was obtained, which was subsequently putted on a hot plate (~250°C). Because of the thermal attenuation along vertical direction from bottom to up of hot plate, a partially reduced GO (P-rGO) was fabricated at the bottom of GO foam, preserving the unaffected and homogeneous GO at the upper section of GO foam. The height of P-rGO in the whole foam was controllable by adjusting thermal treatment time. The thermal treatment time for a-GOM with different ratio of GO to P-rGO (10:1, 1:1 and 0.1:1) is about 5, 60 and 300 s, respectively. Then, forging and pressing treatment made the foam into an asymmetric porous graphene oxide membrane (a-GOM).

Characterization: The morphology of samples was examined by scanning electron microscope (SEM, FLexSEM 1000). Energy-dispersive X-ray spectra (EDX) of the samples was taken on OXFORD (X-Stream-2) unit. The optical photographs were from Camera (Canon EOS 80D). X-ray diffraction (XRD) patterns were recorded on a Bruker AXS D2 PHASER diffractometer with a Cu Kα irradiation source (λ = 1.54 Å). The bottom and top surface of a-GOM was peeled using an adhesive tape for XRD testing. Mechanical property tests were conducted using an Instron 5943 universal testing machine with a strain rate of 0.5 mm min^{-1} for stretching.

Electrical measurements: The output electrical signals of a-GOM were collected using a keithley 2612. The sample was sanwiched between two Au electrodes to record the electrical output performance. An enclosed container is required for the relativity humidity (RH) control by regulating the flow of dry nitrogen or nitrogen of high RH.
The specific surface areas (SSA) of a-GOM is conducted by Methylene blue (MB) adsorption method. The detailed testing process is as below: [s3–5]
A MB aqueous solution (0.2 mg mL^{-1}) was used as the standard probe and we collected the working curve after diluting it for 150, 200, 300 or 600 times.
A piece of a-GOM (1.0 cm× 1.0 cm in size) was immersed in MB solution (2.00 mL, 0.2 mg mL^{-1}) under magnetic stirring for 48 h at room temperature for achieving an adsorption equilibrium. Then, MB solution (15 μL) was got from this system and diluted to 3.0 mL for measuring its light absorbance at 662 nm (U-3010 UV-VIS spectrometer, Hitachi). Finally, the concentration of MB solution at adsorption equilibrium (C_{MB}) can be calculated from its absorbance by referring to the working curve. The SSA of a-GOM was calculated by using following equations:
SSA in area unit (m^2 cm^{-2}) = 2.54× M_{MB} /A (S1)
SSA in mass unit (m^2 g^{-1}) = 2.54× M_{MB} / $M_{a\text{-}GOM}$ (S2)
The constant 2.54 is the literature value of the surface area (m^2) covered by 1.0 mg of adsorbed MB; [s3–5] M_{MB} is the mass change of MB in the equilibrium solution calculated by using the equation of M_{MB} = 0.4 − C_{MB} × (2.00 + 0.15); A is the area of a-GOM, here A=1.0; $M_{a\text{-}GOM}$ is the mass of a-GOM.

Model calculation: The ionic migration mechanism and corresponding induced electric potential are systematically analysed by a theoretical model based on Nernst-Planck-Poisson equations with proper boundary conditions: [s6]

$$\nabla^2\varphi = -\frac{F}{\varepsilon}\sum z_i c_i \quad \text{(S3)}$$

$$j_{i=} - D_i\left(\nabla c_i + \frac{z_i F c_i}{RT}\nabla\varphi\right) \quad \text{(S4)}$$

$$\nabla \cdot j_i = \frac{\partial c}{\partial t} \quad \text{(S5)}$$

where *φ, F, ε, z, c, D, j, R* and *T* represented the electrical potential, Faraday constant, dielectric constant of material, valence of ionic species, ion concentration, diffusion coefficient, ionic flux, ideal gas constant and temperature, respectively. Since the fully hydrated GO can provide extra charge pathways through water adsorbate, we introduce diffusion coefficient and dielectric constant from previous report.[s7] The boundary condition for induced potential on the film surface is described by

$$\vec{n} \cdot \nabla\varphi = -\frac{\sigma}{\varepsilon} \quad \text{(S6)}$$

where *σ* is the surface charge density, which depends on the ionic concentration. Since we aim to simulate the steady state, the ion flux has the zero normal components at the boundaries

$$\vec{n} \cdot j = 0 \quad \text{(S7)}$$

Supplementary Figures

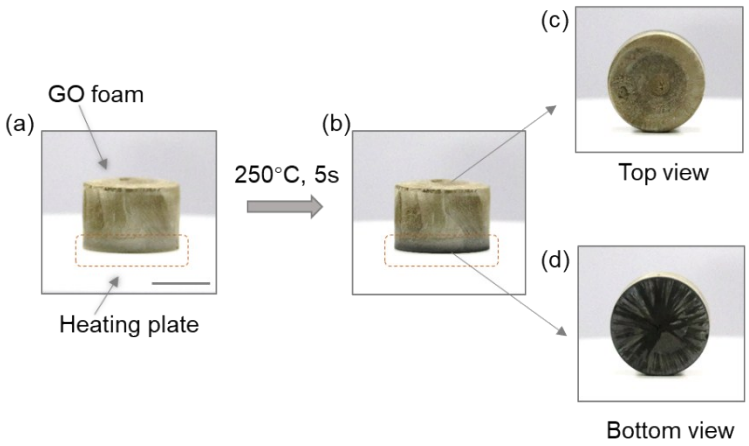

Fig. S1 Photos of directly thermal treatment process on GO foam. (a) GO foam on a heating plate. (b) GO foam after heating at 250°C for 5 s. The bottom surface color of GO foam changes rapidly in the marked red rectangular box. (c) and (d) is the top surface and bottom surface of the foam at c, respectively. Scale bar: a, 1 cm.

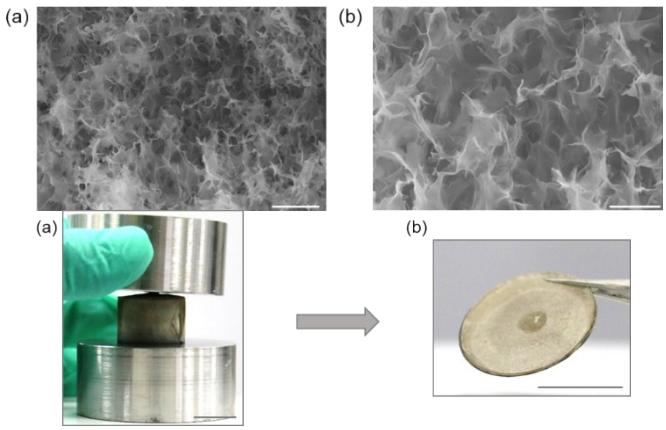

Fig. S2 SEM of GO foam (a) and the enlarged image (b). Scale bars: a, 100 μm; b, 50 μm.

Fig. S3 (a) Forging and pressing treatment on the fabricated foam at Figure S1b. (b) The photo of final a-GOM. Scale bars: a and b, 1 cm.

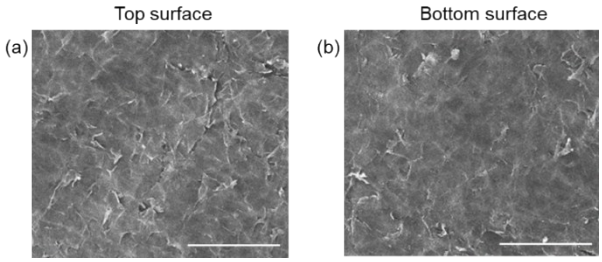

Fig. S4 SEM images of top (a) and bottom (b) surface of a-GOM. Scale bars: a and b, 50 μm.

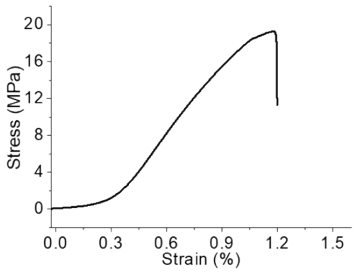

Fig. S5 Strength-strain curve of a-GOM.

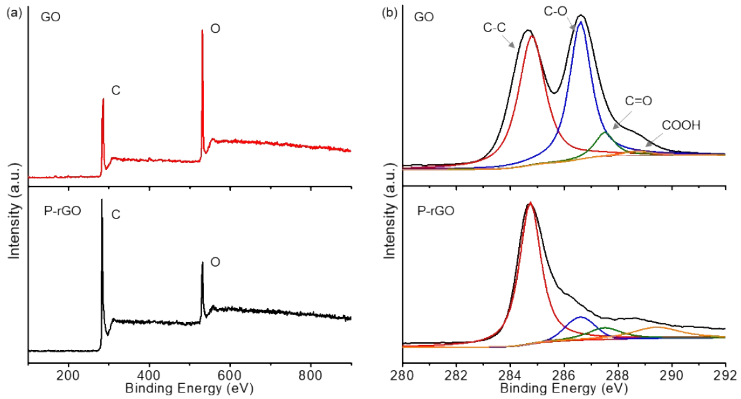

Fig. S6 (a) XPS results of a-GOM on GO and P-rGO surface, respectively. (b) The high-resolution XPS spectrum of C1s peak of GO and P-rGO surface of a-GOM, respectively.

As shown in Fig. S6a, the XPS survey spectrum on GO surface of a-GOM exhibited predominant graphitic C 1s peak at 286 eV and O 1s peak at 532 eV, [s2,s8] the corresponding calculated O/C atomic ratio was about 0.5, which is much higher than that on P-rGO surface (~0.2) of a-GOM. Furthermore, the high-resolution C 1s spectrum (Fig. S6b) of GO surface revealed the presence of C=C/C–C bonding (~284.8 eV), C–O bonding (hydroxyl and epoxy, ~286.6 eV), C=O (carbonyl, ~287.5 eV) and O–C=O bonding (carboxyl, ~288.7 eV).[s2,s8] While P-rGO surface of a-GOM had relatively weaker peaks of oxygen-containing groups after thermal treatment.

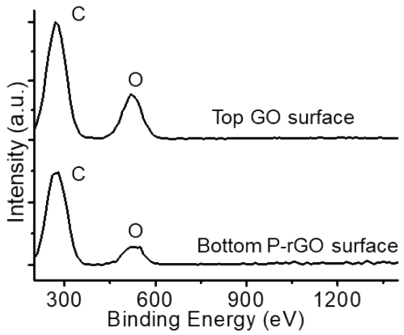

Fig. S7 EDX results of top GO surface and bottom P-rGO surface of a-GOM. The O/C atomic ratio is about 0.5 (GO) and 0.19 (P-rGO), respectively.

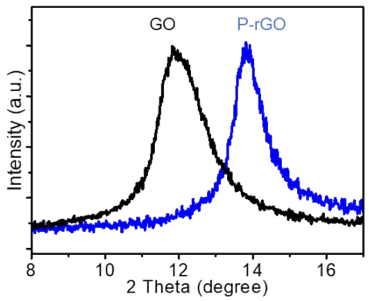

Fig. S8 XRD results of a-GOM on GO (black curve) and P-rGO (blue curve) surface, respectively.

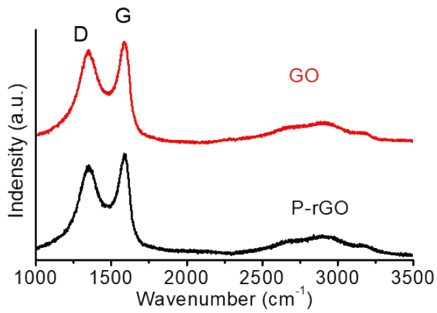

Fig. S9 Raman spectrum of GO and P-rGO surface of a-GOM, respectively.

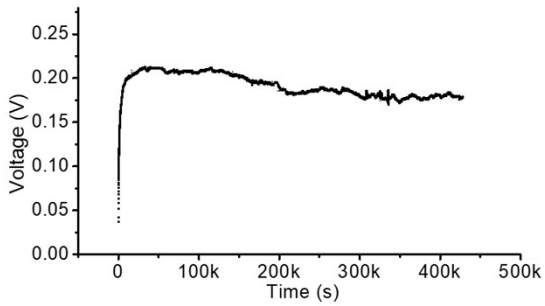

Fig. S10 Open-circuit voltage (V_{oc}) durability test of a-GOM in 100 hours under ambient laboratory conditions with fluctuations of RH between 16% and 26% at room temperature.

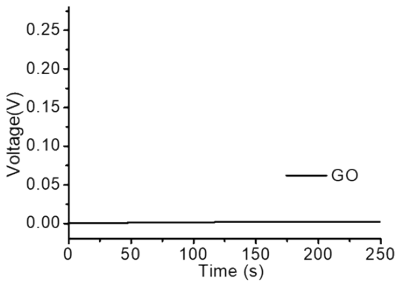

Fig. S11 V_{oc} of pure GO membrane of homogeneous structure.

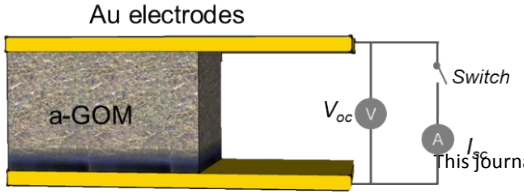

Fig. S12 Testing schematic diagram of V_{oc} and short-circuit current density (I_{sc}) of a-GOM. I_{sc} is detected when connecting the Au electrodes.

Fig. S12–14 demonstrate the recycling power generation process with stable and repeatable V_{oc} and I_{sc} generation. First, the built-in potential of a-GOM induced by its asymmetric structure makes a detected V_{oc} (step i in Fig. S13). Second, by connecting the electrodes with wire, a short-circuit current I_{sc} occurs in the external electric circuit (step ii in Fig. S13). Meanwhile, this process induced current charges both interfaces between a-GOM and two electrodes with electrons and holes, respectively. In this step, I_{sc} increases sharply and then decreases with the charging completed (Fig. S13). At the same time, the charged electrons and holes could form a reverse voltage that should offset the built-in potential of a-GOM. Thus, the detected V_{oc} decays to zero in this step (step ii in Fig. S13). Third, electrodes is disconnected (step iii in Fig. S13). In this step, the electric charges within the interface between a-GOM and electrodes shade away with slowly leakage. Meanwhile, V_{oc} gradually increases to 88% of the initial value but with a slower time (t_2>t_1) because the effect of electric charges in second step (step ii in Fig. S13). This leakage process is also confirmed in Fig. S13, in which the detected V_{oc} of a-GOM also increases slowly after applying a man-induced reverse voltage just like charging process in the second step in Figure S13. Thus, because of the charging and leakage process on a-GOM alone with built-in voltage and current generation process, a-GOM shows favorable electricity cycling generation ability (Fig. S14).

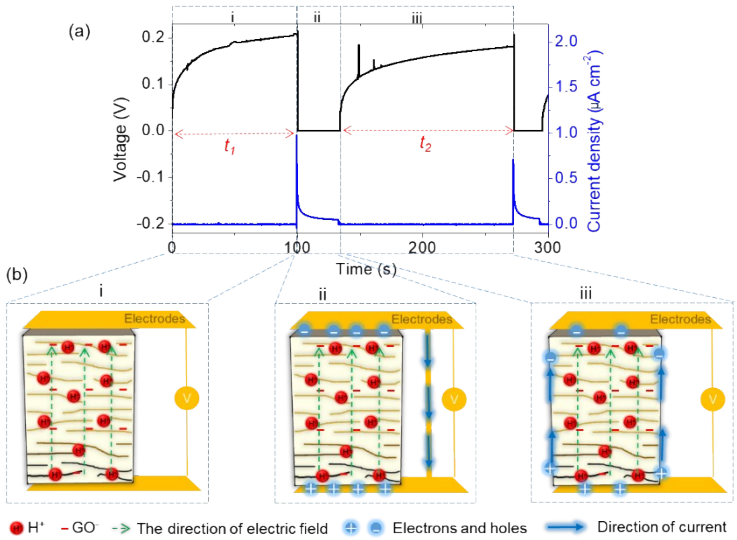

Fig. S13 (a) The detected curves of V_{oc} (black line) and I_{sc} (blue line) of a-GOM, respectively. V_{oc} is detected when disconnecting the Au electrodes in Fig. S11. I_{sc} is detected when connecting the Au electrodes. (b) Schematic diagram of the cycle process of generated voltage and current by a-GOM. The electricity generation cycle is as follows: (i) The built-in potential of a-GOM induced by its asymmetric structure makes a detected V_{oc} (~205 mV). (ii) A short-circuit current I_{sc} occurs in the external electric circuit with the connection of the electrodes in Fig. S11. V_{oc} decays to zero. (iii) V_{oc} recovers with the disconnection of the electrodes.

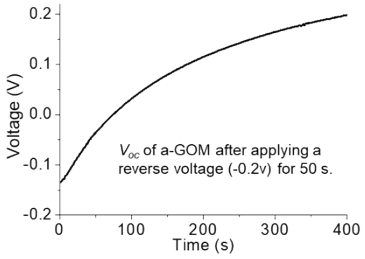

Fig.S14 V_{oc} of a-GOM after applying a reverse voltage (-0.2v) for 50 s.

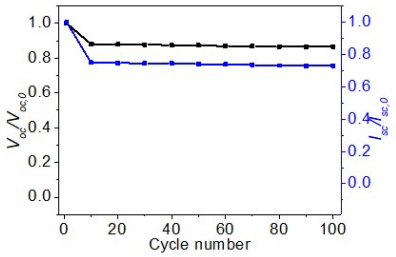

Fig. S15 The detected V_{oc} and I_{sc} cycles of a prototype a-GOM device when contacting and disconnecting electrodes for 100 cycles, respectively.

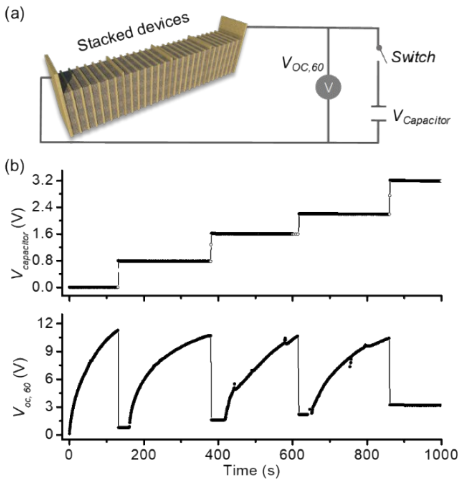

Fig.S16 The voltage of a 10 μF capacitor that is charged using the stacked device with $V_{oc,60}$ of 11.2 V by closing the switch as schemed in (a). As shown in (b), one charge process increases about 0.6–0.9 V ($V_{capacitor}$, up) on capacitor. After four charges, the $V_{capacitor}$ finally reaches to be about 3.2 V.

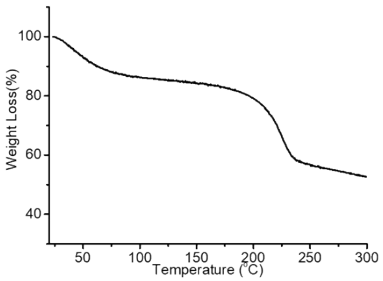

Fig. S17 Thermo Gravimetric analysis (TGA) of a-GOM.

TGA (Fig. S17) showed that a-GOM had mass loss of about 15% around 100 °C due to water removal, which is consistent with previous reports in the literature.[s9]

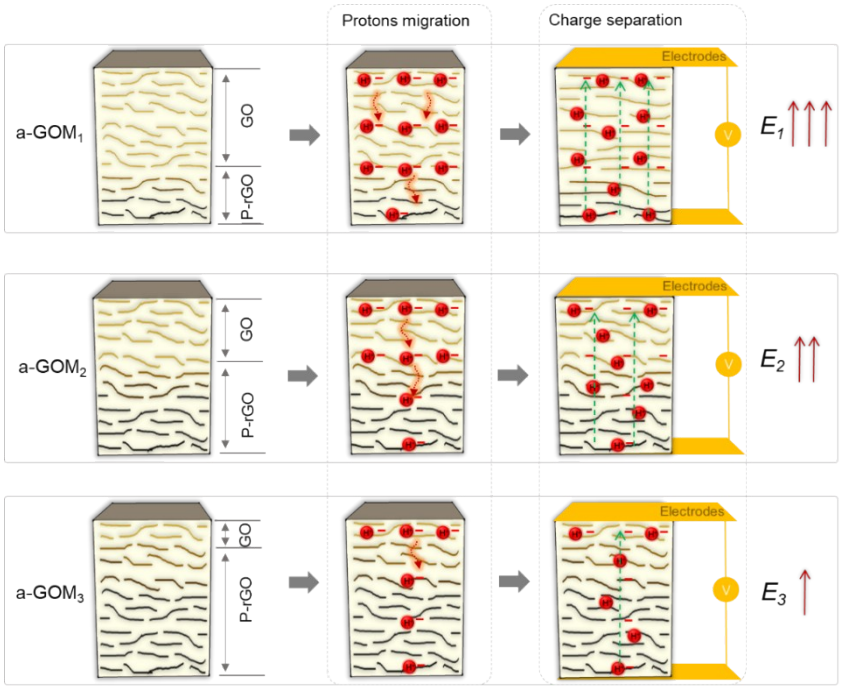

Fig. S18 Thermodynamic analysis of the GO layer influence effect to the generated voltage. From up to down, the radio of GO in a-GOM gradually decrease (a-GOM_1> a-GOM_2>a-GOM_3). E_1, E_2 and E_3 represents the electric field strength generated by a-GOM_1, a-GOM_2 and a-GOM_3, respectively.

When protons migrated from GO to P-rGO section in a-GOM, the inner charge separation induced a directional electric field between two electrodes on a-GOM. Since the area size of electrode is several orders of magnitude larger than the distance between two surfaces of a-GOM in the experimental case, it is reasonable to assume that the two electrodes are infinitely large. From the Gauss theorem, the electric field strength could be described as:[s10]

$E=Q/s\varepsilon_1\varepsilon_0$ (S8)

where the E, Q, s, ε_1 and ε_0 were electric field strength, the amount of charge, the cross-sectional area size of a-GOM, the relative dielectric constants of a-GOM and the vacuum permittivity, respectively. Meanwhile, the electric field could also be defined by

$E=V/d$ (S9)

where V and d were the generated voltage and distance between two electrodes on a-GOM, respectively. Therefore, the final equation is:

$V= Q/ds\varepsilon_1\varepsilon_0$ (S10)

Considering the unchanged chemical composition of a-GOM and environment in experimental case, ε_1 could not affect the final voltage. At the same time, because of the constant value of surface area, distance between two electrodes on a-GOM and the vacuum permittivity, as a result, the generated V is proportional to the amount of charge that could be defined as ionized protons, which were mainly created by oxygen-containing group in GO section of a-GOM in this study.

As schemed in Fig. S18, the protons could decrease dramatically with the reduction of GO section in a-GOM, resulting the weakest electric field (E_3) by a-GOM_3 that had the minimum GO section. To confirm this point, three samples of a-GOM have been fabricated in Fig. S19. The GO section in a-GOM is well regulated by controlling the time of thermal treatment time on primary GO foam (inset Fig. S19). As expected, the generated voltage decreases from 205 to 25 mV along with thinning GO section in a-GOM, confirming the theoretical point mentioned above.

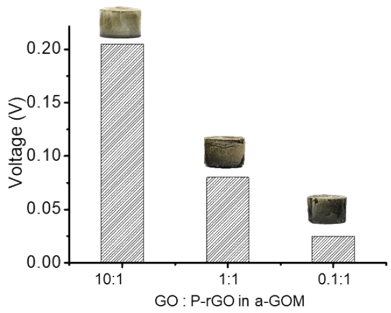

Fig. S19. V_{oc} of a-GOM with different thickness of GO part. From left to right: the ratio of GO to P-rGO in a-GOM is about 10:1, 1:1 and 0.1:1, respectively. Inset is the correspondingly prepared GO foam in the intermediate process, which shows decreased brown GO section from left to right.

The Comsol Multiphysics 4.4 is used to carry out the computation,[s6] and the calculated results are illustrated in Fig. S20. To establish representative model simulating the proposed a-GOM in an affordable computation scale, the 2D models that consisted of two parts representing GO and P-rGO regions with the overall thickness of 120 μm are delineated. The mobile charge was set to positive to show the migration of protons. Such simulation clearly predicts a dependence between the ionic concentration and the proportion of GO thickness. As shown in Fig. S20, the high GO/P-rGO thickness ratio enables higher charge density, thus presenting highest induced potential. When such ratio decreased to 1:1, the charge density is slightly reduced correspondingly, while the induced potential is weakened as well. Regarding the situation that GO/P-rGO thickness ratio reaches down to 1:10, the overall concentration of mobile charge is three orders of magnitude lower than that of 10:1 membrane, and the corresponding induced potential is significantly decreased. Such results are according to our experimental observation, confirming the rationality of the proposed mechanism. Moreover, the predictions also show that the both of the mobile charge density and gradient profile are important for the design of spontaneous electricity generation devices based on materials with well-regulated asymmetric structures in the future.

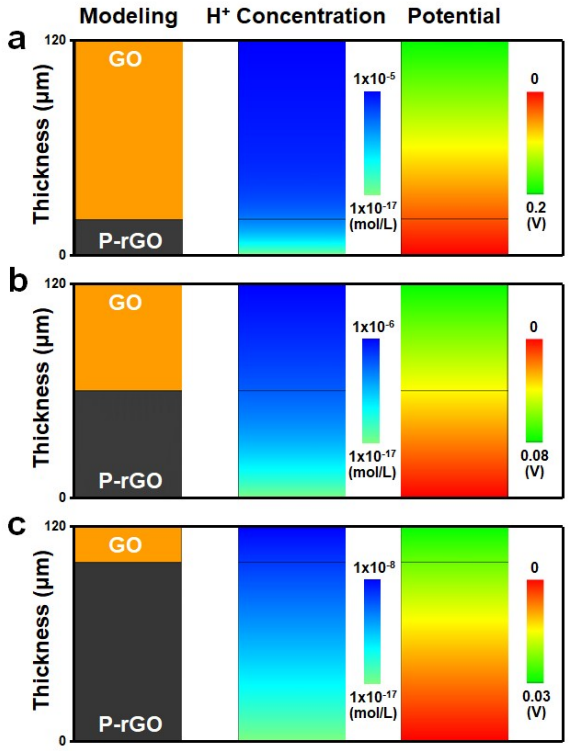

Fig. S20. Modeling, simulated proton distribution and corresponding induced potential of a-GOMs with different thickness of GO part. The ratio of GO to P-rGO in a-GOM is about 10:1 (a), 1:1 (b) and 0.1:1 (c), respectively. The colour maps show the concentration value (from green to blue) and induced potential (from green to red).

s1 H. H. Cheng, Y. X. Huang, Q. L. Cheng, G. Q. Shi, L. Jiang and L. T. Qu, *Adv. Funct. Mater.,* 2017, 1703096.
s2 H. H. Cheng, Z. Fei, J. L. Xue, G. Q. Shi, J. Lan and L. T. Qu, *ACS Nano,* 2016, **10,** 9529.
s3 Y. X. Xu, Z. Y. Lin, X. Zhong, X. Q. Huang, N. O. Weiss, Y. Huang and X. F. Duan, Nat. Commun., 2014, **5**, 4554.
s4 J. Chen, K. X. Sheng, P. H. Luo, C. Li and G. Q. Shi, Adv. Mater., 2012, **24**, 4569–4573.
s5 Q. Q. Zhou, M. M. Wu, M. Zhang, G. C. Xu, B. W. Yao, C. Li and G. Q. Shi, Materials Today Energy, 2017, 6, 181–188.
s6 Q. Liu, Y. Wang, W. Guo, H. Ji, J. Xue and Q. Ouyang, *Phys. Rev. E* 2007, **75**, 051201.
s7 F. Zhao, Y. Liang, H. H. Cheng, L. Jiang and L. T. Qu, *Energy Environ. Sci.,* 2016, **9,** 912.
s8 H. H. Cheng, J. Liu, Y. Zhao, C. G. Hu, Z. P. Zhang, N. Chen, L. Jiang and L. T. Qu, *Angew. Chem. Int. Ed*. 2013, **125,** 10676–10680.
s9 L. J. Cote, R. Cruz-Silva and J. X. Huang, *J. Am. Chem. Soc.* 2009, **131,** 11027–11032.
s10 S. M. Niu, S. H. Wang, L. Lin, Y. Liu, Y. S. Zhou, Y. F. Hu and Z. L. Wang, *Energy Environ. Sci.* 2013, **6,** 3576–3583.

